ORGANIC PROCESS RESEARCH & DEVELOPMENT
OPR&D
Article
Cite This: Org. Process Res. Dev. 2018, 22, 178−189
pubs.acs.org/OPRD

Continuous-Flow In-Line Solvent-Swap Crystallization of Vitamin D_3

Marc Escribà-Gelonch,*[,†] Volker Hessel,[†] Manuel C. Maier,[‡] Timothy Noël,[†] Maria Fernanda Neira d'Angelo,[†] and Heidrun Gruber-Woelfler*[,‡,§]

[†]Eindhoven University of Technology, Department of Chemical Engineering and Chemistry, De Rondom 70, 5612 AP Eindhoven, The Netherlands

[‡]Graz University of Technology, Institute of Process and Particle Engineering, NAWI Graz, Inffeldgasse 13, 8010 Graz, Austria

[§]Research Center Pharmaceutical Engineering GmbH, Inffeldgasse 13, 8010 Graz, Austria

ABSTRACT: A continuous tandem in-line evaporation−crystallization is presented. The process includes an in-line solvent-swap step, suitable to be coupled to a capillary based cooler. As a proof of concept, this setup is tested in a direct in-line acetonitrile mediated crystallization of Vitamin D_3. This configuration is suitable to be coupled to a new end-to-end continuous microflow synthesis of Vitamin D_3. By this procedure, vitamin particles can be crystallized in continuous flow and isolated using an in-line continuous filtration step. In one run in just 1 min of cooling time, ∼50% (w/w) crystals of Vitamin D_3 are directly obtained. Furthermore, the polymorphic form as well as crystals shape and size properties are described in this paper.

1. INTRODUCTION

Crystallization is one of the most important and most commonly used pathways to separate and purify solid materials in chemistry, and especially in the pharmaceutical industry.[1,2] Particle properties such as size, shape, polymorphism, and particle size distribution (PSD) play a pivotal role, since they not only define the crystallization process itself, but also strongly impact the subsequent downstream processes in the context of formulation[3,4] (e.g., filtration, drying, and milling[5]). In addition, the crystallization process can determine eminent properties of a pharmaceutical drug formulation such as its bioavailability and stability.[6]

In May 2015, the Food and Drug Administration (FDA) opened a new era in chemical manufacturing and called on pharma manufacturers and Contract Manufacturing Organizations (CMOs) to begin to switch from batch to continuous production which shall be completed in the year 2025.[7] Beyond this legislative regulatory push, the ACS Green Chemistry Pharmaceutical Roundtable, and thus the pharmaceutical industry, have endorsed the same view and declared (small-scale) continuous manufacturing as top-1 priority.[8] Following this approach, integrated continuous purification and isolation procedures are needed to achieve a full compact end-to-end processing. Process simplification is a demand in integrated flow chemistry,[9] which needs accurate process control.[10,11]

In this paper, a continuous flow crystallization of Vitamin D_3 (VD3) is proposed using a new tandem evaporation−crystallization setup, as an example of process simplification as well as proof of the advantages of crystallization in-flow. In the batch process, VD3 is extracted after synthesis (photochemical reaction) first by removal of unreacted 7-dehydrocholesterol (7DHC).[12,13] The obtained resin can be used without further purification in animal feed. Nevertheless, for food and pharmaceutical use, the resin has to follow additional purification steps to obtain the crystalline form. For this purpose, an esterification of the remaining VD3 provides an alcohol functionality (first step) using organic acids such as propionic, valeric, or butyric acids. Such esters are more readily isolated and crystallized (second step). In the next step, a saponification at max. 80 °C of the purified esters follows, which is performed under alkaline conditions using e.g. a solution of potassium hydroxide in methanol (third step). The isolation of the saponification mixture (fourth step) is carried out by either using VD3 seeds or adding water before extracting with ether. The extracted mixture is then washed sequentially (fifth step) with an aqueous sulfuric or hydrochloric acid, water, a solution of sodium bicarbonate, and ending with water again. After this operation, VD3 is obtained as a resin which still requires further crystallization (sixth step) using an acetone−water solution in a process which can take the order of days.[14] Thus, the isolation of VD3 requires six very long steps in a cascade process.

In a previous study about VD3 crystallization, we described in batch the need for a solvent-swap operation, from the reaction solvent to acetonitrile as the most suited solvent, as a pathway to obtain pure VD3 crystals.[15] The high solubility of VD3 in the reaction solvent, in this case *tert*-butyl methyl ether (*t*-BME),[16] avoids crystallization even at low temperatures. Transferring the solvent-swap concept to the continuous process involves a reaction solvent evaporation combined with a replacement by acetonitrile (solvent B) for the next crystallization step. The constraint of using a solvent swap via solvent evaporation, with the subsequent low pressure, makes the application of segmented flow very difficult. Segmented flow[17] with two immiscible fluids is in addition to the application of ultrasound,[18,19] a rather common way to avoid undesired blockage[20] in continuous applications, since the particles have only little chance for channel wall deposition.[21,22] Other alternatives for small-scale continuous crystallization are mixed-suspension-mixed-product-removal crystallizers (MSMPR) as well as capillaries and tubes in the milli- and

Received: November 2, 2017
Published: December 27, 2017

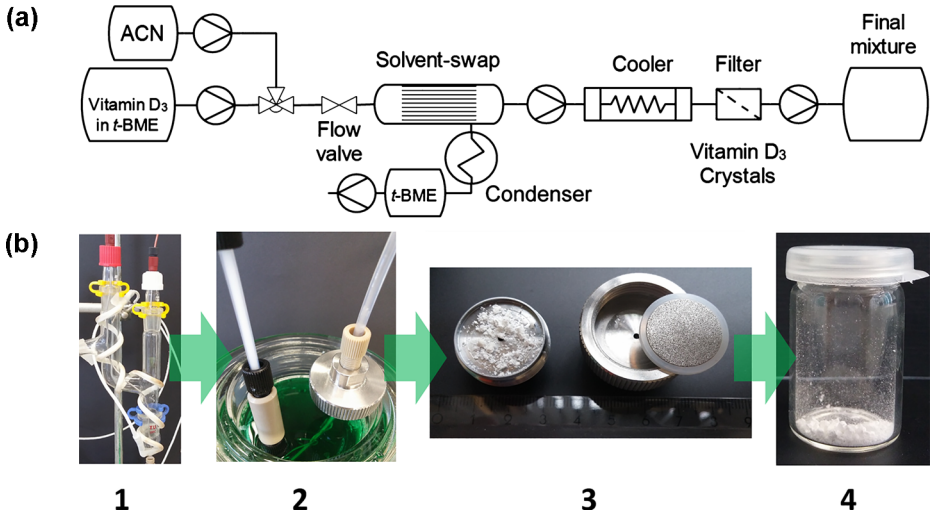

Figure 1. (a) Scheme of the continuous-flow setup used for solvent-swap and crystallization of Vitamin D_3. (b) Detail of the process steps in a single run (1, solvent-swap; 2, cooler and in-line filter; 3, wet crystals on the filter; 4, final dried Vitamin D_3 crystals).

meso-flow[23,24] regime. Prominent examples of this approach are Oslo type crystallizers,[25] draft tube baffle crystallizers,[26] and forced/induced circulation crystallizers.[27] Yet, also these approaches are not practicable with a low-pressure solvent-swap.

In the context of continuous evaporation, only a few microfluidic concepts have been developed, such as membrane-based separation methods, e.g. pervaporation,[28,29] and thin-film evaporation.[30,31] While these approaches are very sophisticated and are based on microfluidic mechanisms (thin-layer evaporation, periodic and chaotic evaporation, and nucleate boiling[32]), in this study a straightforward process in the milli-flow range using droplet evaporation is presented. The latter plays a vital role in various fields of natural science[33] and engineering including cloud physics,[34,35] burning liquid-fuels, air/fuel-premixing, (biological) crystal growth, and painting.[36−38] It allows high heat transfer rates and is therefore used in spray-cooling, in the electronics industry for cooling of integrated circuits, and in inkjet printing as the most common applications.

Thus, a process for tandem evaporation−crystallization including an in-line solvent swap is herewith described and proved for the crystallization of Vitamin D_3. The evaporation and heat exchange are characterized by basic equations. Special emphasis is given on determining the crystal yield and quality, the latter compared to batch results.

2. EXPERIMENTAL SECTION

2.1. Process Description. *Single-Cycle Operation.* The continuous-flow setup used for the solvent-swap and subsequent crystallization is schematically shown in Figure 1.

A solution of 0.22 M Vitamin D_3 (Alfa Aesar, 99% Lot: 10186907) in *tert*-butyl methyl ether (*t*-BME; Alfa Aesar, 99%) is pumped through an IDEX PEEK tube Ora 1/16" ID (0.55 mm) to a T-mixer and mixed with acetonitrile (ACN; Merck >99.9%). *t*-BME is the photoreaction solvent currently in use (solvent A). The VD3 concentration is set according to the maximum solubility of 7DHC in *t*-BME used in the photoreaction (0.22 mol/L).[16] Using pure VD3 assumes that unreacted 7DHC has been removed completely after the photoreaction to Vitamin D_3 and the content of other byproducts is negligible.

The VD3 solution with the corresponding *t*-BME−ACN ratio (A/B) crosses a flow valve (needle valve) to go to the solvent-swap step. The function of this flow valve is to counterbalance the vacuum forces derived from the solvent switch step and to ensure the constant flow rate. The solvent-swap step is shown in more detail in Scheme 1. The device for the solvent swap is made out of glass, vertically placed, and kept at 40 °C using an internal thermocouple (Mohr & CO - Laborhandelsgesellschaft mbH) and an external heating tape (Thermocoax Isopad GmbH), and maintained under a constant pressure of 280 mbar, by using a vacuum controller (Büchi Labortechnik AG). Due to the different boiling points of the

Scheme 1. Schematic Drawing of the Solvent-Swap Step (Unscaled)

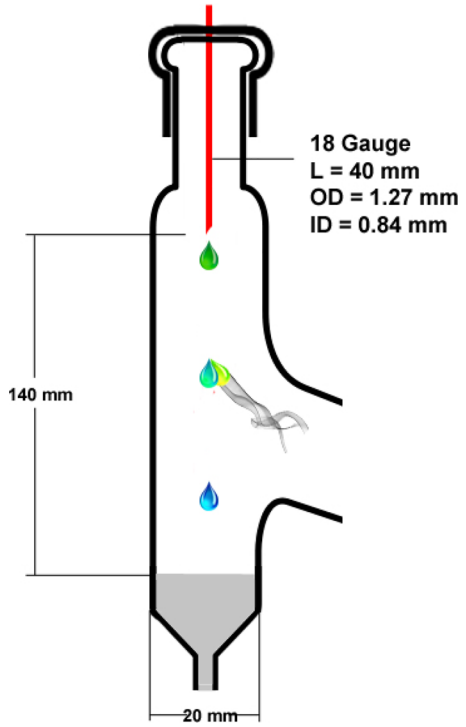

DOI: 10.1021/acs.oprd.7b00351
Org. Process Res. Dev. 2018, 22, 178−189

Scheme 2. Steps of the In-Line Solvent-Swap (Unscaled): (a) in-flight evaporation, (b) droplet crash, and (c) liquid−gas evaporation on the surface liquid

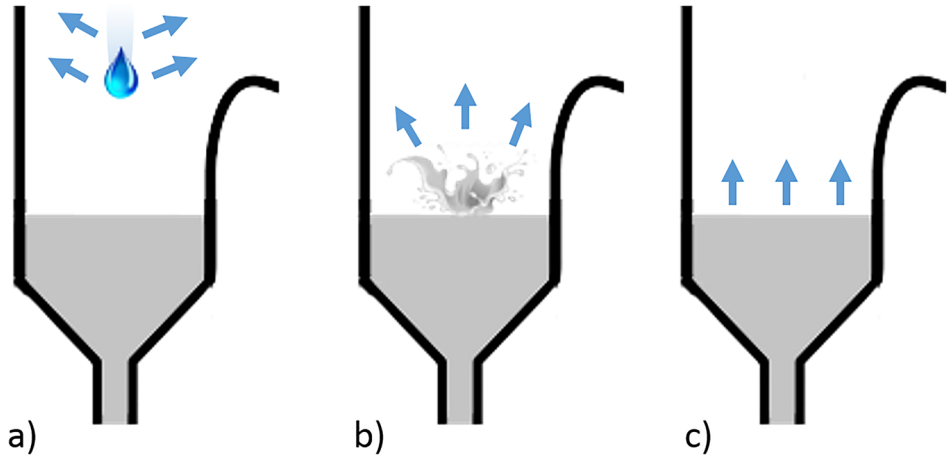

solvents, selective droplet evaporation happens during the falling down of the drops and on the surface of the receptacle placed below the capsule, leaving the VD3 in solvent B. *t*-BME is then condensed in a separate flask. Such evaporation is enhanced by the circular shaped vapor envelope formed around the drop during the fall, which increases the exchange surface strengthening both heat and mass transfer.[39] In short, fast evaporation in the swap capsule happens because of the synergistic interaction of (i) temperature, (ii) pressure, and (iii) in-fly exchange area enhancement. As a result of supersaturation, the solution becomes turbid in this step. The efficiency of the evaporation was checked evaluating the content of the condensed fraction using Shimadzu apparatus Model GC-2010 Plus (SGE-BPX5 6, 0.25 mm ID, 1.0 μm coated column), which indicated that in this operation a 10% (w/w) loss of acetonitrile is assumed to achieve less than 10% of *t*-BME after evaporation.

The supersaturated mixture (see Figure 1) is pumped further on using two microperistaltic pumps (mp6 micropump, Bartels Mikrotechnik GmbH) in order to counterbalance the vacuum forces on the liquid. The solution is transported in this manner in a perfluoroalkoxyalkane (PFA) 1/8" OD capillary tube (1.55 mm ID DuPont High purity) which acts as precooling zone at room temperature. After this step, the capillary containing the supersaturated VD3 solution is submerged in an ethylene glycol (Unil Opal) cooling bath (Endocal RTE-110) with a temperature of 7 °C. Cooling of the supersaturated VD3 solution stimulates crystal formation and growth. The crystals are separated from the solution afterward via a 10 μm pore stainless steel in-line filter (IDEX A-330). The final mixture after the VD3 filtration (see Figure 1) contains also a certain amount of VD3 according to its solubility in ACN at the temperature set in the cooler.

Multicycle Operation. To mimic a recycling procedure, the final ACN mixture (permeate from the previous cycle) is subsequently used as feed for the next cycle. The solution is mixed with a new 0.22 M Vitamin D_3-*t*-BME solution. As a consequence, due to the extra vitamin amount contained in the recycled ACN mixture, the concentration of the solution mixtures in the subsequent cycles are higher than the concentration of the solution in the first cycle. This fact enhances even more supersaturation in the following cycles. In order to know exactly the vitamin concentration in each cycle, the concentration of VD3 in the recycled ACN solution is previously obtained using HPLC measurements (Shimadzu UFLC-XR; GraceSmart RP 18 5μ, 150 mm × 4.6 mm; 100% acetonitrile). After each cycle a mass balance of the Vitamin D_3 in each fraction is carried out. The masses of the solid parts (filtered, permeated, and residues in the cooling coil) are determined after drying the samples overnight under *vacuo* in a desiccator, and the samples for further experiments are stored in the dark at −20 °C under inert gas (nitrogen).

2.2. In-Line Solvent-Swap Operation. The solvent-swap operation is based on the selective in-line evaporation of *t*-BME in three substeps as shown in Scheme 2: (a) in-flight evaporation, (b) droplet crash, and (c) liquid−gas evaporation on the surface liquid on the receptacle placed below. The main aim of this process is to enhance the evaporation surface as much as possible in order to intensify the mass transfer, and subsequently the evaporation. During the formation and the fly of the droplets, a thin layer of saturated vapor is formed around the droplet, generating an energy transfer during the evaporation process. Hence, the evaporation of the components creates concentration gradients in the liquid phase. Since the cavity is thermally controlled at 40 °C, the process is considered as isothermal, and consequently mainly mediated by the mass transfer. The latter is enhanced by the suction effect of the pump, which keeps the pressure at 280 mbar, generating and keeping constant the driving force for the droplet vapor transfer. During the drop formation, evaporation of *t*-BME is possible, but also a mass input because of the flow. For this reason, the content of the solvents is considered almost stable before the drop falling.

The evaporation of in-fly droplets has been previously investigated.[40,41] Tripathi[39] modeled the evaporation of a falling drop and how the shape of the drop as well as the microdroplets, generated behind the droplet by the spray effect of the fall, are changing over time (Scheme 2a). As a consequence, the volume is redistributed and the shape of the drop tends to elongate generating a shaped envelope all around the droplet of a liquid−vapor interface, which is increased in time. Also, the evaporated mass in the envelope enhances the mass transfer within the droplet which changes the density of the droplet. During the flight, the weak interface generated at the upper part, i.e., microdroplets, increases the evaporation surface and subsequently the evaporation rate.

DOI: 10.1021/acs.oprd.7b00351
Org. Process Res. Dev. 2018, 22, 178−189

Hence, despite being the shortest step, the evaporation rate here is the maximum. The 2.6 times difference of the vapor pressures of the involved solvents at 40 °C, 587.3 and 222.2 mbar for *t*-BME[42] and ACN[43] (at atmospheric pressure) respectively, also contributes to the selectivity of the evaporation solvent. In the working conditions (40 °C and 280 mbar), the difference between the partial pressures is even ten times: 255 and 25 mbar for *t*-BME (solvent A) and ACN (solvent B) respectively (calculated with Aspen plus v.9, Aspen Technology Inc.). Therefore, solvent A evaporates 10 times faster than solvent B. In addition, the partial pressures are 2.5 and 9 times (solvents A/B) below the corresponding vapor pressures, respectively.

Immediately after the fly, the droplet crashes to the liquid surface generating again secondary droplets, which enhances the mass transfer as well (Scheme 2b) because the surface is also increased. After the crash, the droplet is diluted in the ACN-VD3 solution. Here the concentration is diffused and the remaining *t*-BME (solvent A) is mixed in the first upper layers of the liquid, and therefore evaporated due to the pressure/temperature conditions. In order to obtain a rough approximation for the difference between the in-fly operation rate (Scheme 2a) and the surface operation rate (Scheme 2c), the following theoretical approach is proposed. As a simplification, the mass transfer within the droplet is neglected and the density of the droplet is considered as constant. Subsequently, assuming a spherical droplet, its volume (V) and consequently its diameter (d_b) are related to the number of moles of its constituents (n_A, n_B, n_C) according to the following expression, where MW refers to the molecular weight and ρ to the density, with A, B as the solvents involved (*t*-BME and ACN) and C as the VD3:

$$V = \frac{1}{6}\pi d_b^3 = \frac{m_{total}}{\rho_{mixture}} = \frac{n_A \cdot MW_A + n_B \cdot MW_B + n_C \cdot MW_C}{\rho_{mixture}} \quad (1)$$

Rearranging eq 1 results:

$$d_b^3 = \frac{6}{\pi \cdot \rho_{mixture}} \cdot (n_A \cdot MW_A + n_B \cdot MW_B + n_C \cdot MW_C) \quad (2)$$

During the decay of the droplet, its diameter is reduced due to partial evaporation of its constituents. Assuming that the density of the droplet does not change significantly during this process, eq 2 can be written as follows:

$$3 \cdot d_b^2 \cdot \frac{d(d_b)}{dt} = \frac{6}{\pi \cdot \rho_{mixture}} \left(MW_A \frac{dn_A}{dt} + MW_B \frac{dn_B}{dt} + MW_C \frac{dn_C}{dt} \right) \quad (3)$$

At this point, some simplifications can be assumed in eq 3 for the purposes of this study. First, due to one of the components of the mixture (i.e., C) being unable to evaporate under the conditions of this experiment (i.e., $\frac{dn_C}{dt} = 0$), eq 3 can be further reduced accordingly. Second, if the mole balance of A and B in the spherical particle assuming isothermal conditions is derived, the accumulation of each component in the droplet equals the mass transfer rate of such a component from the droplet to the gas phase (concentration C) through the gas–liquid interfacial area (A_{GL}). Additionally, the interfacial mass transfer rate is characterized by the overall mass transfer coefficient k_{GL} expressed in units of $m^3_G/(m^2_i \cdot s)$. In eq 4, the concentrations of A and B in the vapor are assumed constant under stable conditions.

$$\frac{dn_A}{dt} = -k_{GL} \cdot A_{GL} \cdot (C_A^{sat} - C_A)$$
$$\frac{dn_B}{dt} = -k_{GL} \cdot A_{GL} \cdot (C_B^{sat} - C_B) \quad (4)$$

Assuming ideal gas law, and including the relation between interfacial area and bubble diameter ($A_{GL} = \pi \cdot d_b^2$), the expressions 4 can be as described respectively in eq 5, where P^{sat} is the vapor pressure.

$$\frac{dn_A}{dt} = -k_{GL,A} \cdot \pi \cdot d_b^2 \cdot \frac{P_A^{sat} - P}{RT}$$
$$\frac{dn_B}{dt} = -k_{GL,B} \cdot \pi \cdot d_b^2 \cdot \frac{P_B^{sat} - P}{RT} \quad (5)$$

By recombining eq 3 with 5, eq 6 can be obtained.

$$\frac{d(d_b)}{dt} = \frac{-2 \cdot k_{GL}}{RT\rho_{mixture}} (MW_A \cdot (P_A^{sat} - P) + MW_B \cdot (P_B^{sat} - P)) \quad (6)$$

Then, the interfacial mass transfer rate is characterized by the overall mass transfer coefficient (k_{GL}) expressed in units of $[m^3_G/(m^2_i \cdot s)]$. The mass transfer coefficient k_{GL} is determined using the Brauer[44] correlation (eq 7).

$$\frac{k_{GL} \cdot d_b}{D_{i,gas}} = 2 + 0.015 \left(\frac{v d_b \rho}{\mu} \right)^{0.89} \left(\frac{\mu}{D_{i,gas}\rho} \right)^{0.7} \quad (7)$$

Therefore, the depletion of solvents A and B in the droplet can be correlated with the size of the droplet and the velocity of the droplet, which for a free falling droplet in vacuum is $v = g \cdot t$, giving eq 8. The mathematical solution of eq 8 was obtained using Matlab (R2015a Academic Use) and describes the in-fly evaporation.

$$\frac{d(d_b)}{dt} = \frac{-2 \cdot D_{i,gas} \left(2 + 0.015 \left(\frac{9.8 \cdot t \cdot d_b \rho}{\mu} \right)^{0.89} \left(\frac{\mu}{D_{i,gas}\rho} \right)^{0.7} \right)}{d_b \cdot RT\rho_{mixture}} [MW_A(P_A^{sat} - P) + MW_B \cdot (P_B^{sat} - P)] \quad (8)$$

Concerning the evaporation on the surface once the droplet is submerged in the liquid, eq 9 gives the expression of the rate of ether evaporation (N) ($mol \cdot m^{-2} \cdot s^{-1}$) dissolved in the very first layers of the mainly solvent B solution placed in the receptacle. In eq 9, c refers to concentration, P and T are the pressure and temperature in the evaporation chamber respectively, L is the height of the chamber, and R is the gas constant.

$$N_A = \frac{c \cdot D_{i,gas}}{L} \ln \left(\frac{P - P_A}{P - P_A^{sat}} \right) = \frac{P \cdot D_{i,gas}}{R \cdot T \cdot L} \ln \left(\frac{P - P_A}{P - P_A^{sat}} \right) \quad (9)$$

Since the p,T conditions in the evaporation chamber are constant and considering that every evaporated molecule is transferred to the cooler of the condenser, the evaporation ratio could be considered almost constant.

Both substeps of the solvent swap are plotted in Figure 2, where a comparable volume reduction of the droplets is shown. Hence, it can be concluded that the evaporation rate during the in-fly step (0.17 s) is 100 times faster than the comparable

DOI: 10.1021/acs.oprd.7b00351
Org. Process Res. Dev. 2018, 22, 178–189

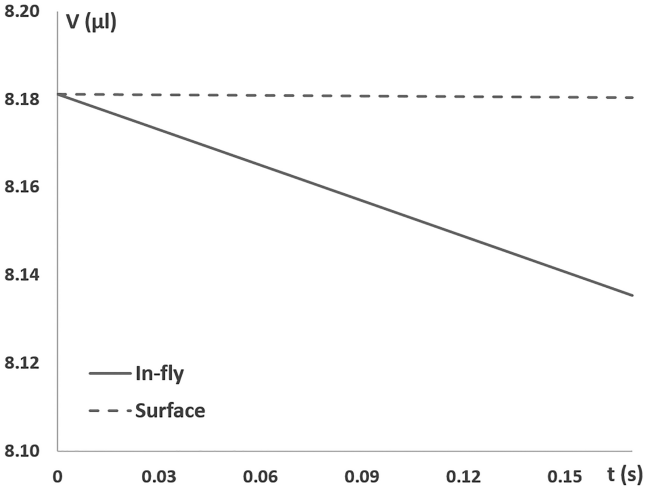

Figure 2. Calculated equivalent drop volume evaporation.

evaporation on the surface, where the solution becomes basically a VD3 solution in acetonitrile. Additionally, a simulation of the solvents evaporation on the surface was performed using Aspen plus v.9 (Aspen Technology Inc.), adjusting all thermodynamic properties according to Mato et al.[45] For an initial ratio of 1:3 v/v % A/B, 96:4 w/w % A/B in the gas phase and 4:96 w/w % A/B in the liquid phase were obtained.

These theoretical approaches were checked experimentally using the evaporation−crystallization setup. Due to the lower solubility of VD3 in the solvent B, supersaturation is reached in the receptacle and the solution becomes opaque after 5 min. The whole evaporation process reaches 20% of the initial droplet volume. This could mean that one-third of evaporation is taken in-fly in just 0.17 s. The flow rates of the pumps were adjusted according to the cooling flow-rate needed in the cooler to set the 1 min cooling time. In addition, the composition of the final solution after the evaporation step was determined experimentally using gas chromatography (Shimadzu GC-2010 Plus). The results show that using 1:3 A/B (v/v), >90 wt % of A can be removed at 40 °C and 280 mbar including a 10 wt % loss of B. The slight difference between the simulation and the experimental results can be explained by the interaction of the solvents with the dissolved VD3.

2.3. Process Temperature Profile. In our crystallization process, the temperature plays a critical role, as the solubility of Vitamin D_3 is strongly temperature dependent.[15,46] Thus, an accurate prediction of the temperature profile during the process is essential. Herewith, the temperature is analyzed from the solvent-swap cavity, where supersaturation takes place, and followed along the cooler. Out of the swap chamber, where the temperature is monitored and kept constant at 40 °C, two additional steps are considered: (i) the precooling section which includes the peristaltic pumps between the solvent swap and the cooler, and (ii) the cooler itself. In the precooling section, heat transfer by conduction (φ_k) and by convection (φ_h) are considered as shown in eq 10. In these equations h (599 W/m^2·K)) and k (0.213 W/m·K) are the convection and conduction coefficients respectively, c_p is the ACN heat capacity (2.2 J/g·K), and L is the wall thickness of the capillary (0.81 mm). For these calculations, laminar flow in the circular tube (Nusselt number = 4.36) was considered, assuming only acetonitrile as solvent B. The acetonitrile parameters were considered as an average, since they do not change so much in the range of temperatures taken into account. In addition, ΔT_1 in eq 10 refers to the difference between the environment temperature and the external wall of the coil (convection). Analogously, ΔT_2 is the difference between the internal and the external side of the coil (conduction) and ΔT_3 is the difference between the internal side of the coil and the solution inside it. As a simplification, the single-operation calculation for each of the two cooling steps was performed without considering heat conduction with the connected parts. In practice, this effect was reduced as much as possible by insulation.

$$\varnothing_h = \varnothing_k = Q;\ h \cdot A \cdot \Delta T_1 = k \cdot L \cdot \Delta T_2 = \dot{m} \cdot C_p \cdot \Delta T_3 \qquad (10)$$

Considering the first two sides of eq 10, the temperature of the wall can be calculated. In the precooling section the wall temperature is 312.5 K and in the cooler it is 293 K. This suggests that the internal wall is almost at the same temperature of the internal mixture. Then, considering the last two sides of

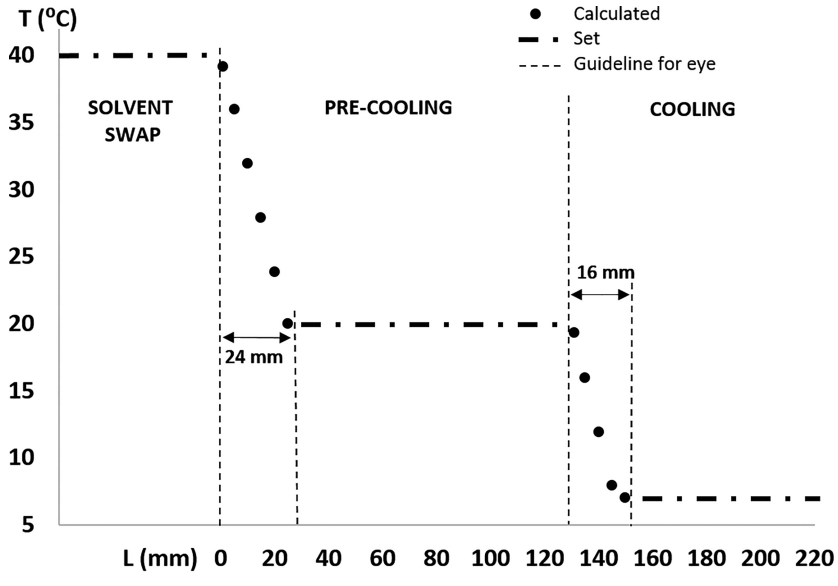

Figure 3. Calculated process temperature profile in the crystallization unit using a flow rate of 15 mL/h.

DOI: 10.1021/acs.oprd.7b00351
Org. Process Res. Dev. 2018, 22, 178−189

eq 10, the dropping temperature can be calculated. Figure 3 plots the temperature profile (*Y*-axis) from the solvent-swap cavity, crossing the peristaltic pumps in the precooling section as well as the cooling operation, along the length of the capillary (*X*-axis). Discrete values refer to the calculation of cooling down. The constant temperature (processing) period is assigned to be the desired set value. The time periods for cooling down are revealed by guidelines for the eye. The precooling section corresponds to the length of the coil at room temperature (20 °C) between the swap cavity and the cooler, and the cooling section, to the length submerged in the cooler. As shown in Figure 3, due to the high heat transfer of the capillary tubes and the low volume inside the capillary, the target temperature is set in the very first sections of the tubing for each step: after the 24 mm tube length in the precooling section and after the 16 mm tube length in the cooling section. Consequently, despite having a short cooling time, the temperature can be considered to be constant for the whole cooling process.

2.4. Crystals Analysis. *Particle Size, Shape, Crystallinity.* The obtained Vitamin D_3 crystals were analyzed using a Leica DM4000 M microscope (50× magnification) with an integrated digital camera. X-ray diffraction (XRD) crystals analysis was carried out with a Rigaku Geigerflex Bragg−Brentano Powder Diffractometer with nickel filtered Cu Kα radiation (λ = 0.1542 nm), performed with 0.02 step in the 2θ range of 0°−90°, and a dwell time of 2 s operating at 40 kV and 30 mA. Peak fitting was performed after background subtraction. Subsequent crystal morphology analysis was characterized using a Scanning Electron Microscope (SEM) JEOL JSM-7401F. Raman data were obtained using a PerkinElmer Raman Station 400 F. The exposure time was 1 s, and the number of exposures was 10. Sampling Super Macro Point (7 points), the wavelength range investigated was 200−3278 cm^{-1} with an interval of 2 cm^{-1}.

Particle Size Distribution. The particle size distribution of the obtained Vitamin D_3 crystals was measured as a suspension in water using a drop of Tween20 as tenside with a HELOS/KR Laser diffraction sensor equipped with a CUVETTE wet dispersion system by Sympatec GmbH (cuvette size: 50 mL, stirring speed: 1000 rpm, optical concentration: 1%−20%, measuring range: combined R2+R5 (0.45−875 μm), evaluation mode: Fraunhofer approximation, software: WINDOX 5.6.0.0).

Particle Purity. In order to evaluate the purity of the obtained crystals and thus ensure that no decomposition of the VD3 occurred, 1.25 mg of commercial and obtained crystals were dissolved in 1.5 mL of acetonitrile and injected in the HPLC instrument (Shimadzu UFLC-XR) with a GraceSmart RP 18 5μ column (150 mm × 4.6 mm), using 100% acetonitrile (99% Merck) as the mobile phase and a UV−visible Shimadzu diode array detector (RID-10A) at 190 nm.

3. RESULTS AND DISCUSSION

3.1. Single-Cycle Experiments. *3.1.1. Residence Time vs Temperature Influence. Choice of Flow Rate.* Since the flow rate of the photochemical reaction was fixed with 15 mL/h, the same flow rate was applied for the crystallization process in order to allow the integrated flow system finally work with one pump. A 1/8" ID (1.55 mm) PFA tubing of 130 mm length was used in the cooler. The reason for the dimensional choice of the capillary diameter was to allow high heat transfer, while having it set sufficiently large to avoid particle-related problems. The dimensional choice of the capillary length is based on the photochemical reaction and crystallization times, being somewhat shorter than 1 min for the first and exactly 1 min for the latter, respectively.

Motivation and Hydrodynamic Residence Time. We aimed first to determine the right temperature and residence time (capillary length) as well as to check if sufficiently small crystals can be produced and if the crystals are small enough to not disturb the flow or even block the channel. The requirement was that the crystal size is at least 100 times smaller than the channel diameter. As residence time, we calculated the hydrodynamic residence time for an empty capillary using the flow rate of the solvent. This simplification ignores the presence of crystals in the real flow and a possible shrinkage of the capillary diameter due to crystal deposition on the walls. Both effects would decrease the real residence time of the solvent. Yet ignoring both effects seems to be justified, since the particle loading is low (4% given as mg crystals/mg solvent in 1:3 *t*-BME/ACN ratio) and the amount of deposited crystals in the capillary diameter is estimated to be <0.4 wt % (as known from some tests on cut samples). The residence time calculated thus is assumed to be characteristic for the real solvent flow and the cooling process enabled through the latter. The residence time, however, is not characteristic for the formed and flowing crystals which may have a different residence time than the flow, probably slower.

Choice of Temperature. The crystallization was first studied at temperatures of 0, 5, 10, 15, and 20 °C using a residence time of 1 min (0.13 m capillary length). With these experiments, a very narrow temperature range of operation was determined: above 10 °C, no crystals were retained in the filter; below 5 °C, the capillary was clogged. Thus, 7 °C was finally used to carry out the crystallization. The mean diameter of the crystals produced in this way was <10 μm. Thus, the milli-capillary size was at least 155 larger which should ensure an undisturbed flow, if agglomeration can be prevented.

Choice of Residence Time. It was therefore aimed to use longer residence times which might allow a larger temperature range. The residence time was adjusted by varying the lengths of the capillary. The latter were set to 0.13, 0.25, and 1.00 m, corresponding to theoretical residence times of 1, 2, and 7.54 min, respectively (flow rate was 15 mL/min). Yet, the use of longer residence times than 1 min was not helpful, as plugging occurred in the longer flow passages. This happened typically in the first third of the longer capillary.

Experimental Reference Conditions. Overall, with a PFA tubing of 130 mm and 1.55 mm ID and a flow rate of 15 mL/h, a residence time of 1 min was used, and a temperature of 7 °C was chosen in all further experiments. With these parameters, a very fast crystallization of Vitamin D_3 was achieved.

3.1.2. Effect of Solvents Ratio. We assumed that the solvent A−solvent B ratio is a pivotal parameter for the crystal size and crystallization speed as well as for the agglomeration. Different ratios were studied using a temperature of 7 °C and the above-defined standard conditions (see Table 1). The amount of VD3 in different fractions was determined: *filtered* as desired and retained as value product, *permeated* through the filter and dissolved to be recycled and refed in the flow, and the amount *deposited* on the capillary walls which is lost for further processing (see also Experimental Section, 2.1). All three fractions are referred to the total VD3 load introduced. The results in Table 1 show a consistent mass balance, as all three fractions (recuperation) are above 90%.

DOI: 10.1021/acs.oprd.7b00351
Org. Process Res. Dev. 2018, 22, 178−189

Table 1. Mass Balance, Crystal Yield, and Process Efficiency at Different Solvent A–Solvent B Ratios

t-BME/ACN	Mass Balance (% w/w)			Crystal Yield (% w/w)	Process Efficiency (% w/w)
	Permeated	Filtered	Deposited		
1:1.5	13	23	59	23	33
1:2	22	36	42	36	60
1:3	34	53	12	53	74
1:4	54	32	7	32	35

As shown in Table 1, two parameters were taken for further optimization: The crystal yield is identical to the filtered amount. It is the crystal mass filtered divided by the total initial VD3 mass (eq 11). The process efficiency is the crystal mass filtered divided by the total initial VD3 mass minus the dissolved amount at 7 °C (eq 11). It thus defines a crystal yield which is corrected with the solubility of VD3 in the solvent, i.e. the amount of crystals filtered off as referred to all molecules which principally (thermodynamically) could crystallize. Following the terminology of "yield", the process efficiency is a kind of "selectivity". The calculated efficiency is a minimum possible value, because it does not include particles below 10 μm, which cannot be retained by the filter. Thus, in reality the efficiency is higher.

$$\text{Yield (\%)} = \frac{\text{mg VD3 filtered}}{\text{initial mg VD3}}$$

$$\text{Efficiency (\%)} = \frac{\text{mg VD3 filtered}}{\text{initial mg VD3} - \text{mg VD3 soluble}} \quad (11)$$

For the single cycle experiments, the highest crystal yield and process efficiency were 53% and 74% for a starting solvent mixture of 1:3 *t*-BME/ACN, respectively. This was considered as a proof of principle, since achieving 100% crystallization yield is not possible, even when using another solvent B, as there is always a fraction of VD3 dissolved in such solvent B.

The solubility of VD3 in ACN was determined to be 8 mg/mL at 7 °C.[15] This is about 10% of the possible crystal load (84 mg/mL). This fraction is for processing the inaccessible and not a big issue, as the permeate can be recycled. This solvent B solubility will, however, become especially relevant when low amounts of the vitamin are used, as then its share and the amount of recycling steps greatly increase. Thus, the continuous crystallization process developed is usable for high VD3 concentrations which are typical for chemically intensified flow chemistry, however, not for diluted flows.

Interestingly, the solvent B (ACN) addition to the solvent A (*t*-BME) results in an antagonistic effect, as shown in Table 1. An increasing amount of the solvent B, on one hand, promotes crystallization, but on the other hand also dissolves increasing amounts of VD3. Thus, the yield of VD3 exhibits a maximum with a solvent A–solvent B ratio of 1:3. The permeated fraction increases because of the higher amount of VD3 dissolved in ACN. Furthermore, the amount of crystals deposited in the capillary decreases when a higher proportion of solvent B is added. The reason therefore is either a lower concentration leads to less clogging or crystals themselves become smaller and thus are less prone to crystal agglomeration. At high solvent B share, also the increased solubility simply cleans the crystals attached to the capillary.

Hence, in the way supersaturation is increased (and the solvent B amount decreases), more crystals are retained in the system, which reduces the filtration efficiency and, consequently, the final yield. Nevertheless, when the solvent B ratio is increased too much, the solubility losses become relevant and the amount of crystals in the filter decrease.

3.2. Multicycle Experiments. While a high crystal yield could be reached in one run, the given analysis has shown that recycling is needed, even under better and best performance. Therefore, this is investigated here and up to three cycles were considered at the standard processing conditions. In addition to the three shares of VD3, its concentration in the permeate is given in Table 2. As shown, the final concentration of the permeated fraction after each cycle remains almost constant, but above the amount corresponding to the solubility of the Vitamin in ACN at 7 °C. This is attributed to particles with a diameter below 10 μm which are smaller than the pores of the filter and just pass through. As the permeated fraction was not thermostated at 7 °C, those crystals redissolved at the higher temperature.

For the 1:3 (v/v) ratio of the starting solvent mixture, the filtered share (crystal yield) decreases, while it increases for the 1:4 ratio. The deposited and permeated share behave conversely in the capillary. The shares of the second and third circle match better than the first one, which could be indicative of increased process stability. The recuperation of this mass balance has an average around 90%.

The 1:4 case thus gives better performance (more crystal yield) because of two effects: the higher starting concentration due to mixing of additional VD3 to the inflow through recycling. This changed concentration necessitates a higher acetonitrile share in the solvent mixture which provides a higher supersaturation, i.e., the driving force for nucleation. Additionally, the efficiency is almost stable using 1:4, which could be set at ~55% per run.

Table 2. Multicycle Experiments at 7 °C and 1 min Cooling Time

t-BME/ACN ratio	Cycle	VD_3[a] in ACN (mg/mL)	Mass Balance (%)			Yield (%)	Efficiency (%)
			Permeated	Filtered	Deposited		
1:3	1	–	34	49	15	49	69
	2	10	24	41	18	41	52
	3	9.5	24	42	20	42	53
1:4	1	–	56	29	7	29	55
	2	10.5	38	38	12	38	55
	3	9.5	42	37	14	37	53

[a]Remaining VD3 added from the permeated ACN of the previous cycle.

DOI: 10.1021/acs.oprd.7b00351
Org. Process Res. Dev. 2018, 22, 178–189

Furthermore, the initial concentrations for each cycle were determined according to the experimental data provided in Table 2, giving the results shown in Table 3. For these values,

Table 3. Concentrations (mg/mL) in Multicycle Experiments at 7 °C with 1 min Cooling Time

	t-BME/ACN ratio (v/v)	
cycle	1:3	1:4
1	28	21
2	38	32
3	37	33

the amounts of VD3 dissolved in the recycled solvent B solution and therefore mixed with a fresh solution of VD3 in solvent A were considered. In light of the results shown in Table 3, and taking into account the highest yields shown in Table 2, we could conclude that the optimal concentration of VD3 for this operation is in the range of 30−35 mg/mL. This range is also quite narrow, since lower concentrations (e.g., 21 mg/mL) would lead to lower yields, because more VD3 is dissolved. Unfortunately, higher concentrations also give more VD3 deposited on the capillary, which also leads to higher losses.

3.3. Crystals Characterization. *3.3.1. Purity of the Crystals.* Cholecalciferol (VD3) can be unstable and degrade in the presence of oxygen and humidity,[47] but also because of operation conditions. This lack of stability may be detected using HPLC analysis. To study the final purity of the vitamin particles after the process, the crystals obtained were compared with a commercial VD3 using HPLC and the protocol described in paragraph 2.4. As a result, a high level of purity fully comparable with the commercial Vitamin D_3 was achieved as shown in Figure 4. In addition, some experiments were

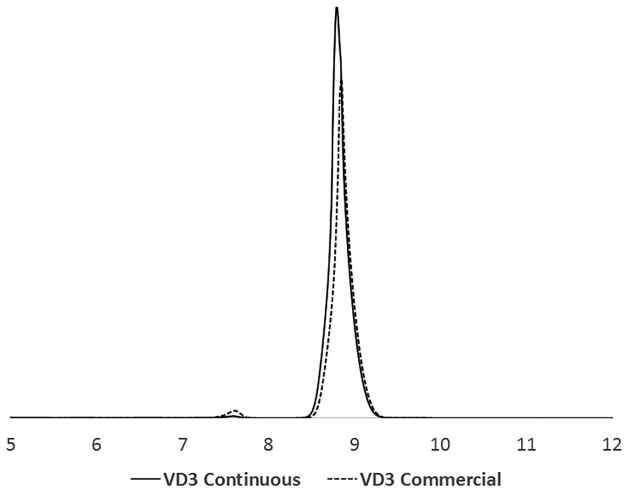

Figure 4. Fragment of overlapped HPLC chromatogram (190 nm) of Vitamin D_3, as obtained in this paper (straight line) and from commercial sample (dotted).

carried out in anhydrous conditions using dried and deoxygenated solvents, in order to test the VD3 stability. For this purpose, ACN was refluxed for 2 h with $CaCl_2$ prior to distillation. The same procedure was used for *t*-BME using $MgSO_4$ as a drying agent. In both solvents, dry nitrogen was passed through for a few minutes for deoxygenation. The experiments in anhydrous and deoxygenated conditions did not show any degradation of VD3.

3.3.2. Crystal Polymorphism. The polymorphic form of the obtained crystals (7 °C, 1 min cooling time) was analyzed using both XRD and Raman spectroscopy using the devices described in 2.4 and were referred to the forms A and B described by Wang et al.[48] We previously reported the possibility to obtain separately form A and form B in batch conditions using solvent B (ACN) and temperature <15 °C.[15] Commercial VD3 was analyzed and correlated with form A. Form B was also correlated in batch with fast processing and low crystallization temperatures. Using the continuous process herewith reported (Figures 5 and 6), the obtained VD3 crystals analysis gives mainly Form B, however also with a small fraction of Form A. In the XRD plot (Figure 5) form B signals can be found at 3.54°, 6.16°, and 9.44°, while form A ones are found in 4.74°, 5.06°, and 6.62°. In addition, the Raman spectrum of the obtained crystals (Figure 6) shows both, form B and form A signals between 2700 and 3000 cm^{-1}. According to our experiments in batch, form A is formed when the starting temperature is higher than 20 °C. Hence, the presence of form A in the crystals obtained in the continuous process could be explained because of the conditions in the solvent-swap step, which operates at 40 °C in order to enhance the evaporation.

3.3.3. Particle Shape and Particle Size Distribution. The crystal habit depends not only on the internal structure of the crystals but also on the growth conditions. For continuous processing the crystal habit takes an important role, because it can easily affect the rheological properties as well as the filtration efficiency of the process. Accordingly, the VD3 crystals obtained with the continuous setup (7 °C, 1 min cooling time) were analyzed using light microscopy and scanning electron microscopy (SEM) described in 2.4. Figure 7 shows a comparison between the particle sizes obtained using the continuous process (upper) and the commercial particles (lower). As it can be seen in the graph, the new particles here obtained are prismatic and smaller than the commercial ones (Alfa Aesar, 99% Lot: 10186907). The latter is quantified in Figure 8. The mean size of the continuous obtained particles is around 10 times smaller (~16 μm) than the commercial VD3 (~114 μm). It can be assumed that the smaller size is due to the fast crystallization conditions, which is correlated with a short crystals growth time. Such small crystals would be preferred in continuous-flow crystallization in order to guarantee the flowability and avoiding undesired clogging. In addition, the wide distribution of the particles obtained with this continuous process can be explained because of some damages during the recovery operation on the filter.

CONCLUSIONS AND OUTLOOK

A continuous tandem in-line evaporation−crystallization was designed and tested with the crystallization of Vitamin D_3. By using this procedure as well as the knowledge of the research group in direct Vitamin D_3 crystallization in batch using ACN,[15] it is possible to avoid the amorphous state of the vitamin (yellow resin). The proposed method achieves the objective of an integrated, simple and intensified process, using shorter times as well as a much lower amount of chemicals. The necessary solvent change was successfully achieved using a solvent-swap cavity especially designed to converge temperature, pressure, and spray effect due to drop falling.

By applying this configuration in the case of Vitamin D_3 crystallization, the solvent A/B (*t*-BME/ACN) ratio of 1:3 (v/

DOI: 10.1021/acs.oprd.7b00351
Org. Process Res. Dev. 2018, 22, 178−189

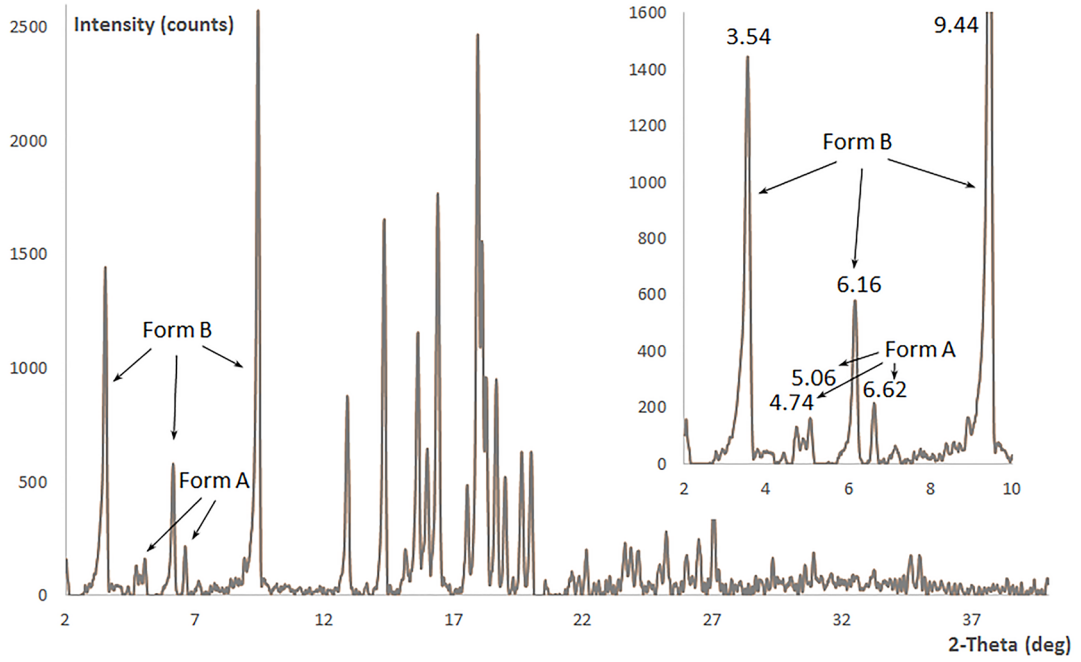

Figure 5. XRD spectra of the Vitamin D_3 crystals obtained in a continuous flow operating at 7 °C during 1 min cooling time.

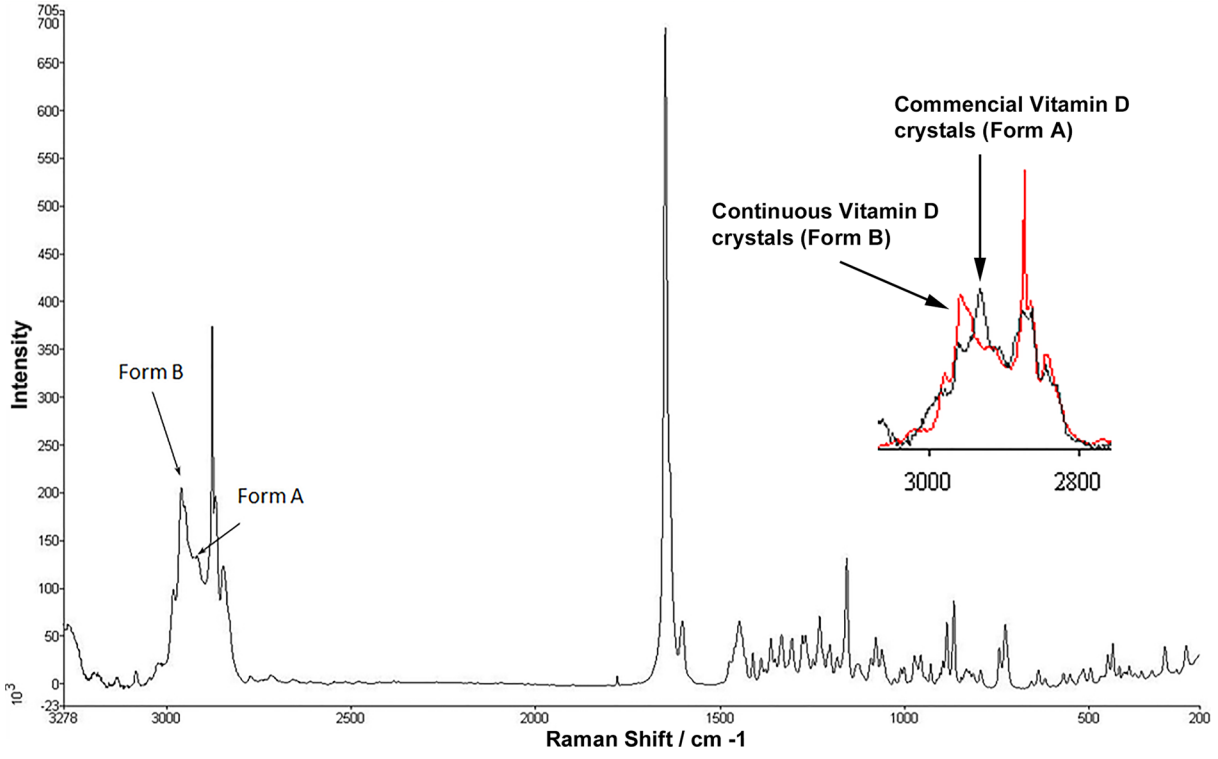

Figure 6. Raman spectrum of the Vitamin D_3 crystals obtained in a continuous flow operating at 7 °C during 1 min cooling time.

v) led to the highest crystal yield and crystal efficiency, the first referring to the total Vitamin D_3 content and the second to the Vitamin D_3 content amenable for crystallization (as part of it dissolves still in the solvent B), respectively. For the higher ratio of 1:4 enhanced dissolution by the solvent B is given. A crystallization yield of 53% is obtained in one run operating at 7 °C during just 1 min of cooling time, yet still below what theoretically would have been possible, but with very short process times. Therefore, multicycle experiments simulated a recycling process, by re-entering the outflowing permeate solution in another (separate) experiment. These experiments showed that a 1:4 (v/v) ratio is more advantageous because of the higher flowability of the crystals in the capillary. The second and third cycle match in their performances, giving an indication that stable performance might be given from here onward.

The continuous process showed polymorphism yielding a mixture of form A and B, with B being the most prevalent

DOI: 10.1021/acs.oprd.7b00351
Org. Process Res. Dev. 2018, 22, 178−189

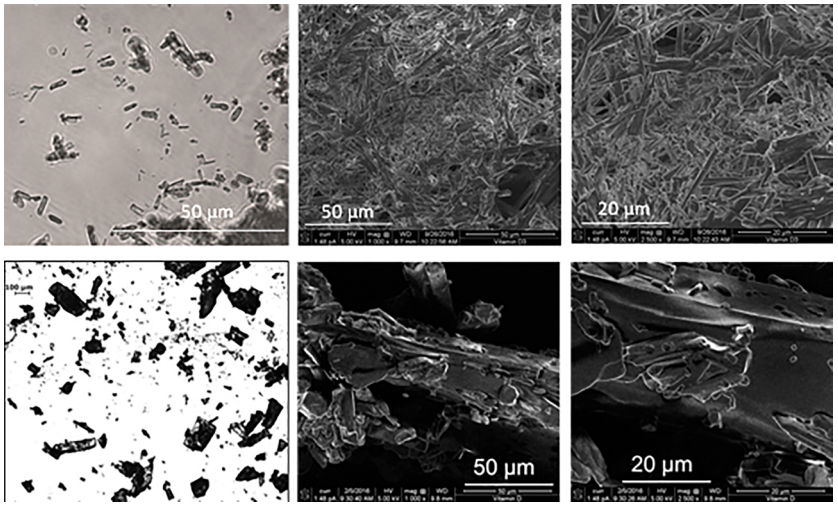

Figure 7. Microscope and SEM pictures of continuous Vitamin D_3 crystals (top) obtained operating at 7 °C during 1 min cooling time, compared with commercial Vitamin D_3 (bottom).

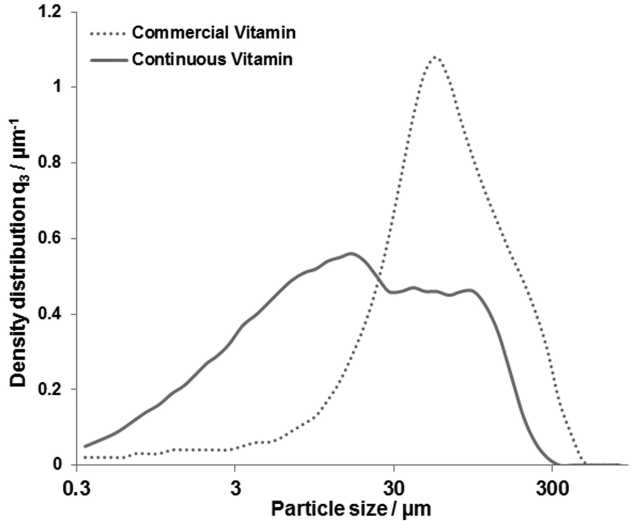

Figure 8. Particle size distribution of Vitamin D_3 crystals obtained operating at 7 °C during 1 min cooling time, compared with commercial Vitamin D_3 (Alfa Aesar, 99% Lot: 10186907).

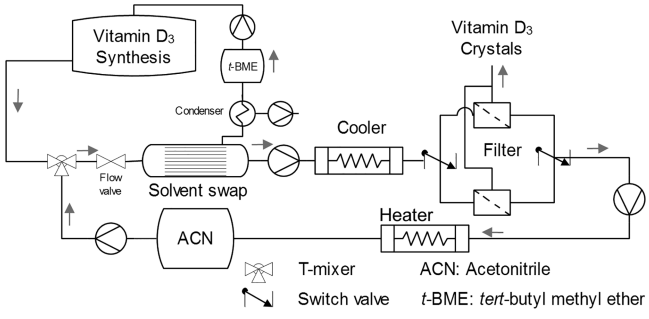

Figure 9. Outlook of the full crystallization setup for medium scale production.

species. The continuously obtained crystals are prismatic and almost 10 times smaller than commercial crystals, which is beneficial for proper, uninterrupted capillary continuous operation.

In light of all the results and process design, an outlook for the crystallization process directly coupled to the syntheses part is shown in Figure 9. After the synthesis module ACN will be added and the solvent-swap discussed in this contribution allows *t*-BME recycling. After the cooler, a flow swap sets an alternative path to the filtration step, allowing an automatic purge system in the nonflowing line. The mixture of Vitamin D_3 and ACN obtained after the filter can be recycled while maintaining the solution at increased temperature in order to avoid undesired precipitations. Thus, the process will allow pure Vitamin D_3 crystals to be obtained while recycling all solvents. Future approaches will concentrate on the applicability of the proposed procedure for Vitamin D_3 and will further investigate the versatility of the novel process for the manufacturing of other APIs.

AUTHOR INFORMATION

Corresponding Authors

*E-mail: m.escriba.gelonch@tue.nl.

*E-mail: woelfler@tugraz.at.

ORCID

Marc Escribà-Gelonch: 0000-0003-0540-7232

Volker Hessel: 0000-0002-9494-1519

Timothy Noël: 0000-0002-3107-6927

Heidrun Gruber-Woelfler: 0000-0002-6917-4442

Notes

The authors declare no competing financial interest.

ACKNOWLEDGMENTS

This project was funded by the Horizon 2020: Marie Skolodowska-Curie Individual Fellowship awarded by Dr. Marc Escribà Gelonch under Grant Agreement Number 659233. The authors also acknowledge Celina Rodrigues de Oliveira for her support as well as the funding granted by the Erasmus program and the mobility program of Graz University of Technology to H.G.-W.

ABBREVIATIONS

7DHC	7-dehydrocholesterol
ACN	Acetonitrile
ACS	American Chemical Society
A_{GL}	Gas−liquid interfacial area

DOI: 10.1021/acs.oprd.7b00351
Org. Process Res. Dev. 2018, 22, 178−189

API	Active pharmaceutical ingredient
c_p	Heat capacity
FDA	Food and Drug Administration
k_{GL}	Mass transfer coefficient
MSMPR	Mixed-suspension-mixed-product-removal crystallizer
MW	Molecular weight
PFA	Perfluoroalkoxyalkane
PSD	Particle size distribution
t-BME	*tert*-Butyl methyl ether
SEM	Scanning Electron Microscope
VD3	Vitamin D_3
XRD	X-ray diffraction

SYMBOLS

V	Volume
d	Diameter
n	Number of moles
MW	Molecular weight
ρ	Density
A	Area
k	Overall mass transfer coefficient
C	Concentration
P^{sat}	Vapor pressure
P	Pressure
μ	Viscosity
D	Diffusivity
R	Gas constant
φ	Heat transfer

REFERENCES

(1) Arsiccio, A.; Barresi, A. A.; Pisano, R. Prediction of ice crystal size distribution after freezing of pharmaceutical solutions. *Cryst. Growth Des.* **2017**, *17*, 4573.

(2) Tung, H. Industrial Perspectives of Pharmaceutical Crystallization. *Org. Process Res. Dev.* **2013**, *17*, 445.

(3) Randolph, A. D.; Larson, M. A. *Theory of particulate process: analysis and techniques of continuous crystallization*; Academic Press: New York, 1988.

(4) Nagy, Z. K.; Braatz, R. D. Advances and new directions in crystallization control. *Annu. Rev. Chem. Biomol. Eng.* **2012**, *3*, 55.

(5) Chow, K.; Tong, H. H. Y.; Lum, S.; Chow, A. H. L. Engineering of pharmaceutical materials: an industrial perspective. *J. Pharm. Sci.* **2008**, *97*, 2855.

(6) Williams, H. D.; Trevaskis, N. L.; Charman, S. A.; Shanker, R. M.; Charman, W. N.; Pouton, C. W.; Porter, C. J. Strategies to address low drug solubility in discovery and development. *Pharmacol. Rev.* **2013**, *65*, 315.

(7) Lee, S. L.; O'Connor, T. F.; Yang, X.; Yu, L. X.; Woodcock, J. Modernizing Pharmaceutical Manufacturing: from Batch to Continuous Production. *J. Pharm. Innov.* **2015**, *10*, 191.

(8) Jiménez-González, C.; Poechlauer, P.; Broxterman, Q. B.; Yang, B. S.; am Ende, D.; Baird, J.; Bertsch, C.; Hannah, R. E.; Dell'Orco, P.; Noorman, H.; Yee, S.; Reintjens, R.; Wells, A.; Massonneau, V.; Manley, J. Key Green Engineering Research Areas for Sustainable Manufacturing: A Perspective from Pharmaceutical and Fine Chemicals Manufacturers. *Org. Process Res. Dev.* **2011**, *15*, 900.

(9) Hessel, V.; Kralisch, D.; Kockmann, N. *Novel Process Windows: Innovative Gates to Intensified and Sustainable Chemical Processes*; Wiley-VCH: Weinheim, 2015.

(10) Hessel, V.; Kralisch, D.; Kockmann, N.; Noël, T.; Wang, Q. Novel Process Windows for Enabling, Accelerating, and Uplifting Flow Chemistry. *ChemSusChem* **2013**, *6*, 746.

(11) Ehrfeld, W.; Hessel, V.; Lowe, H. *Microreactors*; Wiley-VCH Verlag: 2000.

(12) Hirsch, A. L. Vitamin D. *Encyclopedia of Chemical Technology*; John Wiley & Sons: 2000.

(13) Hirsch, A. L. Industrial aspects of Vitamin D. *Vitamin D*; Academic Press: 2011.

(14) Schaaf, K. H.; Schmukler, S.; Klein, H. C. Process for obtaining purified crystalline vitamin D. US3334118, 1967.

(15) Gruber-Woelfler, H.; Escribà-Gelonch, M.; Noël, T.; Maier, M. C.; Hessel, V. Effect of acetonitrile-based crystallization conditions on the crystal quality of Vitamin D3. *Chem. Eng. Technol.* **2017**, *40*, 2016.

(16) Escribà-Gelonch, M.; Noël, T.; Hessel, V. Continuous-flow high-p, T intensification of Vitamin D3 synthesis using a ultraviolet lamp. *Org. Process Res. Dev.* **2017**, DOI: 10.1021/acs.oprd.7b00318.

(17) Lignos, I. G.; Wootton, R. C. R.; DeMello, A. J.; Stone, B. M. Segmented Flow Microfluidics. *Encyclopedia of Biophysics, EBSA*; Springer: Berlin, Heidelberg, 2013; p 2300.

(18) Noël, T.; Naber, J. R.; Hartman, R. L.; McMullen, J. P.; Jensen, K. F.; Buchwald, S. L. Palladium-catalyzed amination reactions in flow: overcoming the challenges of clogging via acoustic irradiation. *Chem. Sci.* **2011**, *2*, 287.

(19) Eder, R. J. P.; Schrank, S.; Besenhard, M. O.; Roblegg, E.; Gruber-Woelfler, H.; Khinast, J. G. Continuous Sonocrystallization of Acetylsalicylic Acid (ASA): Control of Crystal Size. *Cryst. Growth Des.* **2012**, *12*, 4733.

(20) Hartman, R. L.; Naber, J. R.; Zaborenko, N.; Buchwald, S. L.; Jensen, K. F. Overcoming the Challenges of Solid Bridging and Constriction during Pd-Catalyzed C-N Bond Formation in Microreactors. *Org. Process Res. Dev.* **2010**, *14*, 1347.

(21) Liedtke, A. K.; Scheiff, F.; Bornette, F.; Philippe, R.; Agar, D. W.; De Bellefon, C. Liquid-Solid Mass Transfer for Microchannel Suspension Catalysis in Gas-Liquid and Liquid-Liquid Segmented Flow. *Ind. Eng. Chem. Res.* **2015**, *54*, 4699.

(22) Deshpande, J. B.; Kulkarni, A. A. Effect of interfacial mass transfer on the dispersion in segmented flow in straight capillaries. *AIChE J.* **2015**, *61*, 4294.

(23) Besenhard, M. O.; Neugebauer, P.; Ho, C. D.; Khinast, J. G. Crystal Size Control in a Continuous Tubular Crystallizer. *Cryst. Growth Des.* **2015**, *15*, 1683.

(24) Eder, R. J. P.; Schrank, S.; Besenhard, M. O.; Roblegg, E.; Gruber-Woelfler, H.; Khinast, J. G. Continuous Sonocrystallization of Acetylsalicylic Acid (ASA): Control of Crystal Size. *Cryst. Growth Des.* **2012**, *12*, 4733.

(25) Kang, C. L. Krystal-Oslo type crystallizer design. *Gongcheng* **1966**, *39*, 81.

(26) Genck, W. J. Guidelines for crystallizer selection and operation. *Chem. Eng. Prog.* **2004**, *100*, 26.

(27) Wierzbowska, B.; Hutnik, N.; Piotrowski, K.; Matynia, A. *Cryst. Growth Des.* **2011**, *11*, 1557.

(28) Adiche, C.; Sundmacher, K. Experimental investigation on a membrane distillation based micro-separator. *Chem. Eng. Process.* **2010**, *49*, 425.

(29) Matuschewski, H.; Schedler, U. MSE — modified membranes in organophilic pervaporation for aromatics/aliphatics separation. *Desalination* **2008**, *224*, 124.

(30) Ehrfeld, W. *Microreaction Technology: Industrial Prospects SE — 55*; Springer: 2000.

(31) Moschou, P.; de Croon, M.; van der Schaaf, J.; Schouten, J. C. Liquid flow rate effects during partial evaporation in a falling film micro contactor. *Chem. Eng. Process.* **2013**, *69*, 95.

(32) Oron, A.; Davis, S. H.; Bankoff, S. G. Long-scale evolution of thin liquid films. *Rev. Mod. Phys.* **1997**, *69*, 931.

(33) Sazhin, S. S. Modelling of fuel droplet heating and evaporation: Recent results and unsolved problems. *Fuel* **2017**, *196*, 69.

(34) Zhang, H.; Quon, J.; Alvarez, A. J.; Evans, J.; Myerson, A. S.; Trout, B. Development of Continuous Anti-Solvent/Cooling Crystallization Process using Cascaded Mixed Suspension, Mixed Product Removal Crystallizers. *Org. Process Res. Dev.* **2012**, *16*, 915.

(35) Misyura, S. Y. Contact angle and droplet evaporation on the smooth and structured wall surface in a wide range of droplet diameters. *Appl. Therm. Eng.* **2017**, *113*, 472.

DOI: 10.1021/acs.oprd.7b00351
Org. Process Res. Dev. 2018, 22, 178−189

(36) Hu, H.; Larson, R. G. Evaporation of a sessile droplet on a substrate. *J. Phys. Chem. B* **2002**, *106*, 1334.
(37) Maatar, A.; Chikh, S.; Ait Saada, M.; Tadrist, L. Transient effects on sessile droplet evaporation of volatile liquids. *Int. J. Heat Mass Transfer* **2015**, *86*, 212.
(38) Schönfeld, F. Droplet Evaporation. *Encyclopedia of Microfluidics and Nanofluidics*; Li, D., Ed.; Springer: 2008.
(39) Tripathi, M. K.; Sahu, K. C. Evaporating Falling Drop. *Procedia IUTAM* **2015**, *15*, 201.
(40) Hardt, S.; Wondra, F. Evaporation model for interfacial flows based on a continuum-field representation of the source terms. *J. Comput. Phys.* **2008**, *227*, 5871.
(41) Schlottke, J.; Weigand, B. Direct numerical simulation of evaporating droplets. *J. Comput. Phys.* **2008**, *227*, 5215.
(42) Kraehenbuehl, M. A.; Gmehling, J. Vapor Pressures of Methyl tert-Butyl Ether, Ethyl tert-Butyl Ether, Isopropyl tert-Butyl Ether, tert-Amyl Methyl Ether, and tert-Amyl Ethyl Ether. *J. Chem. Eng. Data* **1994**, *39*, 759.
(43) Heim, G. Vapor tensions and latent heat of vaporization of some normal nitriles. *B. Soc. Chim. Belg.* **1933**, *42*, 467.
(44) Brauer, H. *Stoffaustausch einschliesslich chemischer Reaktionen*; Verlag Sauerländer: Aarau, Switzerland, 1971.
(45) Mato, F. A.; Berro, C. Vapor-liquid equilibria and excess volumes for binary systems of methyl tert-butyl ether (MTBE) with trans-1,2-dichloroethylene and acetonitrile. *J. Chem. Eng. Data* **1991**, *36*, 262.
(46) Liang, R.; Bao, Z.; Su, B.; Xing, H.; Ren, Q. Solubility of Vitamin D3 in Six Organic Solvents at Temperatures from (248.2 to 273.2). *J. Chem. Eng. Data* **2012**, *57*, 2328.
(47) Gandi, A. S.; Pilgaonkar, P. S.; Rustomjee, M. T. Stabilized vitamin D formulations. WO2014158033 A1, 2014.
(48) Wang, J. R.; Zhu, B.; Yu, Q.; Mei, X. Selective crystallization of vitamin D_3 for the preparation of novel conformational polymorphs with distinctive chemical stability. *CrystEngComm* **2016**, *18*, 1101.

DOI: 10.1021/acs.oprd.7b00351
Org. Process Res. Dev. 2018, 22, 178−189